Scattering of an evanescent light field by a single cesium atom near a nanofiber

Fam Le Kien,[1,*] V. I. Balykin,[1,2] and K. Hakuta[1]
[1]*Department of Applied Physics and Chemistry, University of Electro-Communications, Chofu, Tokyo 182-8585, Japan*
[2]*Institute of Spectroscopy, Troitsk, Moscow Region 142092, Russia*
(Received 4 October 2005; published 27 January 2006)

We investigate the scattering of an evanescent light field by a single cesium atom outside a nanofiber. We show that the confinement of the field, the presence of the longitudinal field component and the tangential Poynting vector component, the enhancement of spontaneous emission, and the degeneracy of the atomic ground state substantially affect the scattering process. We find that, in the close vicinity of the fiber surface, the transmittance of the field in the stationary regime can be substantially reduced to 48% due to scattering into radiation modes (with the efficiency as high as 44%) and backward guided modes (with the efficiency as high as 8%).

DOI: 10.1103/PhysRevA.73.013819 PACS number(s): 42.50.Nn, 32.70.Jz, 32.80.Pj, 03.75.Be

I. INTRODUCTION

Recently, thin fibers have attracted considerable attention for a wide range of potential practical applications [1,2]. A fiber-based method for *microscopic* trapping and guiding of individual atoms has been proposed [3,4]. The method is based on the use of a subwavelength-diameter silica fiber (nanofiber) with a single (red-detuned) light beam [3] or two (red- and blue-detuned) light beams [4] launched into it. The advantages of the scheme are the following: (i) localization of atoms to a subwavelength region, (ii) high efficiency to detect individual atoms, (iii) high accessibility to the trapped atoms, and (iv) achievement of strong coupling between light and matter.

The control and manipulation of individual neutral atoms in a microscopic optical dipole trap are of great importance for various applications in both fundamental and applied physics [5,6]. The ability to control and manipulate atoms individually may open a way to engineering of the quantum states of small sets of trapped particles, in order to encode and process information at the quantum level [7]. In order to find an effective way to probe, control, and manipulate an atom trapped outside a nanofiber, we need to know the optical response of the atom to a near-resonant field propagating along the fiber.

Absorption and scattering are the usual outcomes of the interaction of an atom with a near-resonant light field. An important characteristic of absorption and scattering is the cross section that can be interpreted as the effective area of the atom for removing radiation from the incident light beam. In the model of a two-level atom interacting with a stationary quasiplane resonant light wave, the cross section of the atom depends only on the transition frequency and is given by $\sigma=3\lambda_0^2/2\pi$ (for the fine-structure transition $J_g=0\leftrightarrow J_e=1$) [8]. Here λ_0 is the wavelength of the atomic transition. It has been shown by Ritsch *et al.* [9] that, due to the transverse confinement of the field in a waveguide, a single atom is able to have a significant effect on a light wave packet. When the transverse extension of the field in a guided mode is close to the radiative cross section of the atom, the latter becomes a significant scatterer. In addition, one might be able to observe a strong-coupling regime, in which the coherent interaction between the guided field and the atom is not masked by damping [9].

The theory of Ritsch *et al.* [9] avoided the precise geometric specifications of the waveguide and the guided mode. It also neglected the modification of spontaneous emission of the atom by the waveguide. However, the thin thickness of a nanofiber and the high contrast between the refractive indices of the silica core and the vacuum clad can substantially modify the polarization properties and intensity distribution characteristics of the field [10,11]. In addition, the presence of the fiber can substantially affect the spontaneous emission process [12,13]. Furthermore, the multilevel structure of a real atom modifies the absorption and scattering characteristics [13,14]. All these factors must be included in a systematic treatment for the interaction of an atom with a near-resonant light field in the close vicinity of a nanofiber.

In this paper, we study the scattering of an evanescent light field by a single cesium atom trapped outside a nanofiber. Using a semiclassical treatment, we show that the confinement of the field, the presence of the longitudinal field component and the tangential Poynting vector component, the enhancement of spontaneous emission, and the degeneracy of the atomic ground state substantially affect the scattering process.

Before we proceed, we note that, due to recent developments in taper fiber technology, thin fibers can be produced with diameters down to 50 nm [1,2]. Thin fiber structures can be used as building blocks in future atom and photonic micro- and nano-devices.

The paper is organized as follows. In Sec. II we describe the model and present the basic equations. In Sec. III we present numerical results. Our conclusions are given in Sec. IV.

*Also at Institute of Physics and Electronics, Vietnamese Academy of Science and Technology, Hanoi, Vietnam.

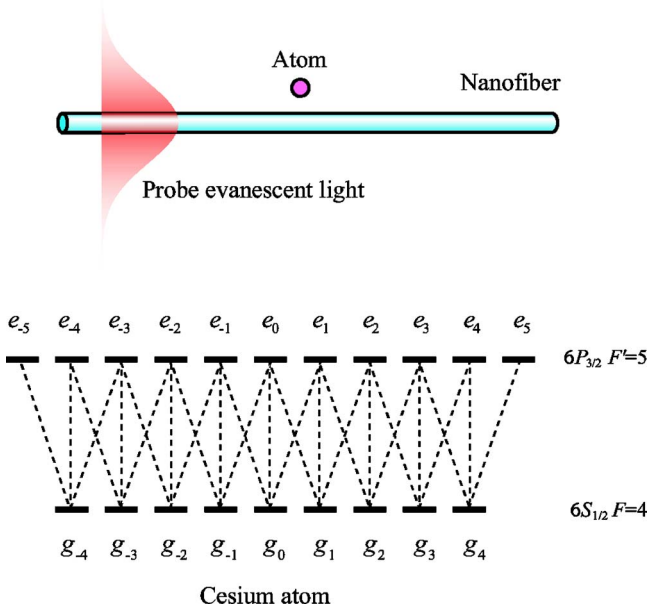

FIG. 1. (Color online) Upper part: Probing an atom by an evanescent light field propagating along a thin optical fiber. Lower part: Schematic of the $6P_{3/2}F'=5$ and $6S_{1/2}F=4$ hyperfine-structure (hfs) levels of a cesium atom.

II. MODEL

Consider a cesium atom trapped outside a thin single-mode optical fiber (see the upper part of Fig. 1). The thin fiber has a cylindrical silica core, with the radius a and the refractive index n_1, and an infinite vacuum clad, with the refractive index $n_2=1$. The trapping can be performed by using a single red-detuned light beam [3] or a pair of red- and blue-detuned laser beams [4]. After loading the atom into the trap, we turn on a weak classical coherent near-resonant continuous-wave light in a fundamental mode of the fiber to probe the atom. This light produces an evanescent field that can be absorbed and then re-emitted into the surrounding environment by the atom. The effect of the trapping fields on the atom at the probing stage can be minimized by reducing the intensities or by using the magic wavelengths [15].

A. Structure of the evanescent light field outside the fiber

We consider the case where the light field is excited by a laser beam that is circularly polarized at the input. For certainty, we assume that the circulation of the field around the fiber axis z is counterclockwise. We introduce the notation ω and $k=\omega/c$ for the frequency and free-space wave number, respectively, of the field. We represent the electric component of the field as $\mathbf{E}=(\boldsymbol{\mathcal{E}}e^{-i\omega t}+\boldsymbol{\mathcal{E}}^* e^{i\omega t})/2$. Outside the fiber, in the cylindrical coordinates $\{r,\varphi,z\}$, the cylindrical components of the envelope vector $\boldsymbol{\mathcal{E}}$ are given by [16]

$$\mathcal{E}_r = i\mathcal{A}[(1-s)K_0(qr)+(1+s)K_2(qr)]e^{i(\beta z+\varphi)},$$

$$\mathcal{E}_\varphi = -\mathcal{A}[(1-s)K_0(qr)-(1+s)K_2(qr)]e^{i(\beta z+\varphi)},$$

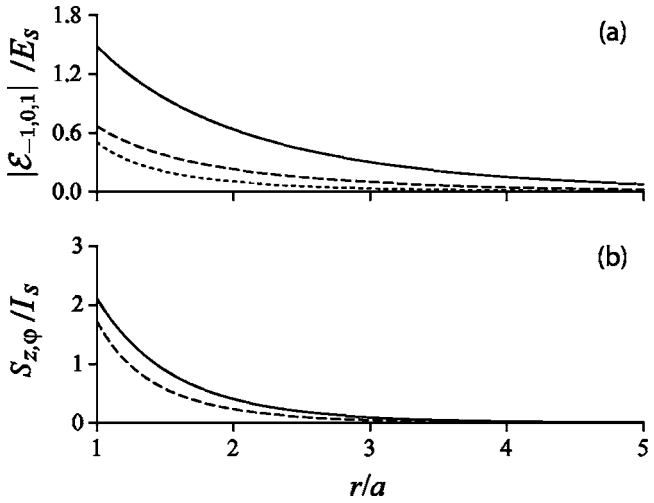

FIG. 2. (a) Spherical tensor components $\mathcal{E}_{-1}$ (solid line), $\mathcal{E}_0$ (dashed line), and $\mathcal{E}_1$ (dotted line) of the electric field, normalized to the saturation field strength $E_s=0.9$ V/cm. (b) Longitudinal component S_z (solid line) and tangential component S_φ (dashed line) of the averaged Poynting vector, normalized to the saturation intensity $I_s=1.1$ mW/cm^2. The refractive indices of the fiber and the vacuum clad are $n_1=1.45$ and $n_2=1$, respectively. The fiber radius is $a=0.2$ μm, the light wavelength is $\lambda=852$ nm, the light polarization is counterclockwise rotating, and the light propagation power is $P_z=10$ pW.

$$\mathcal{E}_z = \mathcal{A}\frac{2q}{\beta}K_1(qr)e^{i(\beta z+\varphi)}. \quad (1)$$

Here β is the longitudinal propagation constant for the fiber fundamental mode, $q=(\beta^2-n_2^2k^2)^{1/2}$ characterizes the decay of the field outside the fiber, and s is defined as $s=(1/q^2a^2+1/h^2a^2)/[J_1'(ha)/haJ_1(ha)+K_1'(qa)/qaK_1(qa)]$, with $h=(n_1^2k^2-\beta^2)^{1/2}$ being a parameter for the field inside the fiber. The coefficient $\mathcal{A}$ characterizes the amplitude of the field. The notation J_n and K_n stand for the Bessel functions of the first kind and the modified Bessel functions of the second kind, respectively.

We introduce the notation $\mathcal{E}_{-1}=(\mathcal{E}_x-i\mathcal{E}_y)/\sqrt{2}$, $\mathcal{E}_0=\mathcal{E}_z$, and $\mathcal{E}_1=-(\mathcal{E}_x+i\mathcal{E}_y)/\sqrt{2}$ for the spherical tensor components of the field envelope vector $\boldsymbol{\mathcal{E}}$. These components are given by

$$\mathcal{E}_{-1} = \sqrt{2}i\mathcal{A}(1-s)K_0(qr)e^{i\beta z},$$

$$\mathcal{E}_0 = \mathcal{A}\frac{2q}{\beta}K_1(qr)e^{i(\beta z+\varphi)},$$

$$\mathcal{E}_1 = -\sqrt{2}i\mathcal{A}(1+s)K_2(qr)e^{i(\beta z+2\varphi)}. \quad (2)$$

We note that, for fundamental modes with counterclockwise rotating polarization of conventional, weakly guiding fibers [16], the components $\mathcal{E}_1$ and $\mathcal{E}_0$ are negligible compared to $\mathcal{E}_{-1}$. However, for subwavelength-diameter fibers, $\mathcal{E}_1$ and $\mathcal{E}_0$ are not negligible at all [11]. We illustrate in Fig. 2(a) the spherical tensor components of the field outside the fiber. The figure shows that, in the close vicinity of

the fiber surface, the three components $\mathcal{E}_{-1}$, $\mathcal{E}_0$, and $\mathcal{E}_1$ are comparable to each other. The effects of these components on the atom are of the same order. Therefore we must include all these components in the calculations for the atomic state.

An important characteristic of the light propagation is the cycle-averaged Poynting vector

$$\mathbf{S} = \frac{1}{2}\,\mathrm{Re}(\boldsymbol{\mathcal{E}} \times \boldsymbol{\mathcal{H}}^*), \tag{3}$$

where $\boldsymbol{\mathcal{H}}$ is the envelope of the magnetic component of the field. We denote the longitudinal, tangential, and radial components of the vector $\mathbf{S}$ in the cylindrical coordinates by the notation S_z, S_φ, and S_r, respectively. For guided modes of fibers, we always have $S_r=0$. In the case of conventional weakly guiding fibers [16], the tangential component S_φ is small compared to the longitudinal component S_z. However, in the case of subwavelength-diameter fibers, the tangential component S_φ is substantial [see Fig. 2(b)]. This component describes the energy flow that circulates around the fiber. The presence of this flow is a consequence of the fact that the longitudinal component of the field in the fundamental mode is not zero.

We note that, since the light field is confined in the fundamental mode of the fiber, a very small power can still produce a substantial intensity in the close vicinity of the fiber surface. Indeed, Fig. 2(b) shows that, although the total power of the z-direction energy flow is as small as 10 pW, the magnitudes of the averaged Poynting vector components S_z and S_φ in the close vicinity of the fiber surface are comparable to the saturation intensity $I_s=2\pi^2\hbar c\gamma_0/3\lambda_0^3=1.1\ \mathrm{mW/cm^2}$ for the cesium D_2 line [17]. Here γ_0 is the upper-level population decay rate of the atom. Similarly, Fig. 2(a) shows that the strengths of the electric-field components $\mathcal{E}_{0,\pm1}$ are comparable to the saturation field strength $E_s=\sqrt{2I_s/c\epsilon_0}=0.9\ \mathrm{V/cm}$ for the cesium D_2 line [17].

The propagation power P_z is determined as the integral of S_z over the transverse plane of the fiber, that is,

$$P_z = \int_0^{2\pi} d\varphi \int_0^{\infty} r S_z dr. \tag{4}$$

The z-axis flux is given by

$$n_z = P_z/\hbar\,\omega. \tag{5}$$

Since the evanescent field $\boldsymbol{\mathcal{E}}$ around the fiber has a substantial longitudinal component $\mathcal{E}_z$, the quantities P_z and n_z do not represent the total amount of energy and the number of photons, respectively, incident into the atom per unit time. These quantities characterize only a part but not the whole field acting on the atom. However, it follows from Gauss's theorem and Poynting's theorem that the propagation power P_z is conserved along an adiabatically tapered fiber, provided the loss of the field is negligible. Therefore P_z can be measured experimentally at the end of such a fiber.

B. Interaction of the atom with the evanescent light field

We now examine the interaction of the cesium atom with the evanescent light field outside the fiber. We consider the hyperfine-structure (hfs) magnetic substates $|FM\rangle \equiv |LSJIFM\rangle$ and $|F'M'\rangle \equiv |L'SJ'IF'M'\rangle$ of a lower state $|LJ\rangle$ and an upper state $|L'J'\rangle$, respectively. Here L, S, J, I, F, and M are the quantum numbers for the orbital electronic angular momentum, electronic spin, total electronic angular momentum, nuclear spin, total atomic angular momentum, and magnetic momentum, respectively. The electronic and nuclear spins of atomic cesium are $S=1/2$ and $I=7/2$. We study the D_2 line, which occurs at the wavelength $\lambda_0=852$ nm and corresponds to the transition from the ground state $6S_{1/2}$ (with $L=0$ and $J=1/2$) to the excited state $6P_{3/2}$ (with $L'=1$ and $J'=3/2$). We assume that the cesium atom is initially prepared in the hfs level $F=4$ of the ground state $6S_{1/2}$ and that the field is tuned close to resonance with the hfs level $F'=5$ of the excited state $6P_{3/2}$ (see the lower part of Fig. 1). Among the hfs components of the D_2 line, the transition $6S_{1/2}F=4 \leftrightarrow 6P_{3/2}F'=5$ has the strongest oscillator strength. The on-resonance scattering cross section for this transition is, in the framework of the perturbation theory and with the assumption about negligible population redistribution, estimated to be about 0.14 $\mu\mathrm{m}^2$ (see the Appendix). Because of the selection rule $\Delta F=0,\pm1$, spontaneous emission from the excited hfs level $6P_{3/2}F'=5$ to the ground state is always to the ground-state hfs level $6S_{1/2}F=4$, not to the other ground-state hfs level $6S_{1/2}F=3$. Therefore the magnetic sublevels of the hfs levels $6S_{1/2}F=4$ and $6P_{3/2}F'=5$ form a closed set, which is used for laser cooling in magneto-optical traps [17].

For convenience, we introduce the notation $e_{M'}$ and g_M for the magnetic sublevels $F'M'$ and FM of the hfs levels $6P_{3/2}F'=5$ and $6S_{1/2}F=4$, respectively. The coupling between $e_{M'}$ and g_M by spontaneous emission and by the spherical tensor components of the evanescent light field is illustrated in the lower part of Fig. 1. For $l=0,\pm1$, the l spherical tensor component of the dipole moment for the transition between $e_{M'}$ and g_M is given by [18]

$$d^{(l)}_{e_{M'}g_M} = (-1)^{I+J'-M'}\langle J'\|D\|J\rangle\sqrt{(2F+1)(2F'+1)} \times \begin{Bmatrix} J' & F' & I \\ F & J & 1 \end{Bmatrix} \begin{pmatrix} F & 1 & F' \\ M & l & -M' \end{pmatrix}. \tag{6}$$

Here the array in the curly braces is a $6j$ symbol, the array in the parentheses is a $3j$ symbol, and $\langle J'\|D\|J\rangle$ is the reduced electric-dipole matrix element in the J basis. For the cesium D_2 line, we have $\langle J'\|D\|J\rangle=6.347\ \mathrm{a.u.}=5.38\times10^{-29}$ Cm [17].

The interaction of the atom with the classical coherent field is characterized by the set of Rabi frequencies

$$\Omega_{eg} = \frac{1}{\hbar}(\mathbf{d}_{eg}\cdot\boldsymbol{\mathcal{E}}) = \frac{1}{\hbar}\sum_{l=0,\pm1}(-1)^l d^{(l)}_{eg}\mathcal{E}_{-l}. \tag{7}$$

Knowing the structure and profile of the field as well as the level structure of the atom, we can easily calculate the Rabi

frequencies (7). Meanwhile, the effects of the vacuum quantum fluctuations of the field around the fiber on the cesium atom are characterized by the set of decay rates [13]

$$\gamma_{ee'gg'} = \gamma^{(g)}_{ee'gg'} + \gamma^{(r)}_{ee'gg'},$$

$$\gamma_{ee'} = \sum_g \gamma_{ee'gg} = \gamma^{(g)}_{ee'} + \gamma^{(r)}_{ee'}. \tag{8}$$

Here the set of coefficients $\gamma^{(g)}_{ee'gg'}$ and $\gamma^{(g)}_{ee'}=\Sigma_g\gamma^{(g)}_{ee'gg}$ describes spontaneous emission into guided modes, and the set of coefficients $\gamma^{(r)}_{ee'gg'}$ and $\gamma^{(r)}_{ee'}=\Sigma_g\gamma^{(r)}_{ee'gg}$ describes spontaneous emission into radiation modes. The explicit expressions for these coefficients are given in Ref. [13]. We note that, in the absence of the fiber, we have $\gamma_{e_ie_jg_kg_l}=\gamma^{(\mathrm{free})}_{e_ie_jg_kg_l}$ and $\gamma_{e_ie_j}=\gamma^{(\mathrm{free})}_{e_ie_j}$, where [19]

$$\gamma^{(\mathrm{free})}_{e_ie_jg_kg_l} = \gamma_0 \sum_{l=0,\pm1} (-1)^{2F+M'_i+M'_j}(2F'+1) \times \begin{pmatrix} F & 1 & F' \\ M_k & l & -M'_i \end{pmatrix} \begin{pmatrix} F & 1 & F' \\ M_l & l & -M'_j \end{pmatrix},$$

$$\gamma^{(\mathrm{free})}_{e_ie_j} = \gamma_0\delta_{ij}. \tag{9}$$

Here $\gamma_0=\omega_0^3|\langle J'\|D\|J\rangle|^2/[3\pi\epsilon_0\hbar c^3(2J'+1)]=33\times10^6\ \mathrm{s}^{-1}$ is the decay rate of the cesium state $6P_{3/2}$ in free space, with ω_0 being the atomic transition frequency.

The diagonal coefficients $\gamma^{(g)}_{ee}$ and $\gamma^{(r)}_{ee}$ describe the population decay from the excited magnetic sublevel $|e\rangle$ into guided and radiation modes, respectively. Their expressions are given by [13]

$$\gamma^{(g)}_{ee} = \frac{2\omega_0\beta'(\omega_0)}{\epsilon_0\hbar}\sum_g |(\mathbf{d}_{eg}\cdot\mathbf{e}^{(\omega_0)})|^2,$$

$$\gamma^{(r)}_{ee} = \frac{2\omega_0}{\epsilon_0\hbar}\sum_g\sum_m \int_0^{k_0n_2} d\beta |(\mathbf{d}_{eg}\cdot\mathbf{e}^{(\omega_0,\beta,m)})|^2. \tag{10}$$

Here $\mathbf{e}^{(\omega_0)}$ is the mode function of a fundamental guided mode that has the resonant frequency ω_0, a fixed (forward or backward) propagation direction, and a fixed (counterclockwise or clockwise) polarization. Similarly, $\mathbf{e}^{(\omega_0,\beta,m)}$ is the mode function of a radiation mode with the frequency ω_0, the longitudinal propagation constant β, the order m, and a fixed (plus or minus) polarization. The mode functions $\mathbf{e}^{(\omega)}$ and $\mathbf{e}^{(\omega,\beta,m)}$ describe the spatial profiles of the vector components of the electric part of the light field in the guided and radiation modes and are given in Refs. [13,16]. The total decay rate of the population of the excited magnetic sublevel $|e\rangle$ is

$$\gamma_{ee} = \gamma^{(g)}_{ee} + \gamma^{(r)}_{ee}. \tag{11}$$

The spontaneous emission characteristics of the atom are modified by the presence of the fiber [12,13]. We illustrate this effect by plotting in Fig. 3 the results of Ref. [13] for the spatial dependence of the spontaneous emission rates of cesium magnetic sublevels into guided modes, radiation modes, and both types of modes. The figure shows that different magnetic sublevels of the same state $6P_{3/2}$ have different decay rates in the close vicinity of the fiber surface, unlike the case of atomic cesium in free space. For the atom on the fiber surface, the parameters $\gamma^{(g)}_{ee}/\gamma_0$, $\gamma^{(r)}_{ee}/\gamma_0$, and γ_{ee}/γ_0 for the set of different M_e are spread from 0.31 to 0.48, from 1.24 to 1.25, and from 1.55 to 1.73, respectively. Clearly, the presence of the fiber produces substantial decay rates into guided modes. As expected, the effect of the fiber on the decay rates is largest for the atom on the fiber surface. When the atom is far away from the fiber, $\gamma^{(g)}_{ee}$ reduces to zero while both $\gamma^{(r)}_{ee}$ and γ_{ee} approach γ_0.

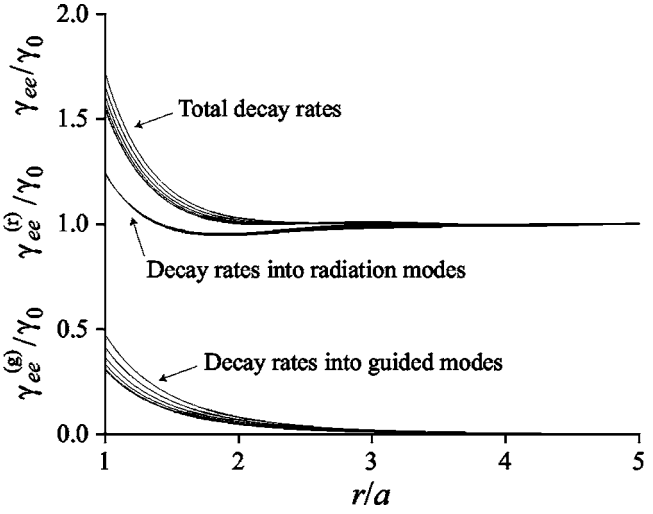

FIG. 3. Spatial dependence of the population decay rates into guided modes, radiation modes, and both types of modes for various magnetic sublevels of atomic cesium. Different lines in each group correspond to different values $|M_e|=0$, 1, 2, 3, 4, and 5. The rates are normalized to the free-space decay rate γ_0. Other parameters are as in Fig. 2.

For a two-level atom with a dipole d_{eg} and a population decay rate γ_e, the on-resonance scattering cross section in the weak-field regime is $\sigma\propto|d_{eg}|^2/\gamma_e$ [see Eq. (A3)]. Therefore we expect that the enhancement of spontaneous emission tends to reduce the ability of the atom to absorb and scatter incident light. Such a reduction is opposite to the increase due to the existence of the longitudinal field component $\mathcal{E}_0$ and the tangential component S_φ of the Poynting vector.

The state of the atom can be characterized by a density operator ρ. The matrix elements of ρ are governed by the equations

$$\dot\rho_{e_ke_l} = \frac{i}{2}\sum_j (\Omega_{e_kg_j}\rho_{g_je_l} - \Omega^*_{e_lg_j}\rho_{e_kg_j}) - \frac{1}{2}\sum_j (\gamma_{e_ke_j}\rho_{e_je_l} + \gamma_{e_je_l}\rho_{e_ke_j}),$$

$$\dot\rho_{g_kg_l} = -\frac{i}{2}\sum_j (\Omega_{e_jg_l}\rho_{g_ke_j} - \Omega^*_{e_jg_k}\rho_{e_jg_l}) + \sum_{i,j}\gamma_{e_je_ig_lg_k}\rho_{e_ie_j},$$

$$\dot{\rho}_{g_k e_l} = -\frac{i}{2}\sum_j \Omega^*_{e_l g_j}\rho_{g_k g_j} + \frac{i}{2}\sum_j \Omega^*_{e_j g_k}\rho_{e_j e_l} - i\delta\rho_{g_k e_l} - \frac{1}{2}\sum_j \gamma_{e_j e_l}\rho_{g_k e_j}. \quad (12)$$

Here, $\delta=\omega-\omega_0$ is the detuning of the field from the atomic transition frequency $\omega_0=\omega_e-\omega_g$. Inserting the Rabi frequencies (7) and the modified decay rates (8) into Eqs. (12) and solving these equations, we can calculate the density matrix of the atom interacting with the field in the vicinity of the fiber.

C. Scattering characteristics

We introduce several useful characteristics for the scattering process. The scattering rate into guided modes $\Gamma^{(g)}_{sc}$, the scattering rate into radiation modes $\Gamma^{(r)}_{sc}$, and the total scattering rate Γ_{sc} are defined as

$$\Gamma^{(g)}_{sc} = \sum_{ee'} \gamma^{(g)}_{ee'}\rho_{e'e}, \quad \Gamma^{(r)}_{sc} = \sum_{ee'} \gamma^{(r)}_{ee'}\rho_{e'e},$$

$$\Gamma_{sc} = \Gamma^{(g)}_{sc} + \Gamma^{(r)}_{sc} = \sum_{ee'} \gamma_{ee'}\rho_{e'e}. \quad (13)$$

The powers scattered (energies scattered per unit time) into guided modes, radiation modes, and both types of modes are $P^{(g)}_{sc}=\hbar\omega\Gamma^{(g)}_{sc}$, $P^{(r)}_{sc}=\hbar\omega\Gamma^{(r)}_{sc}$, and $P_{sc}=P^{(g)}_{sc}+P^{(r)}_{sc}=\hbar\omega\Gamma_{sc}$, respectively. The efficiencies of scattering from the field into guided modes, radiation modes, and both types of modes are characterized by the parameters

$$\eta^{(g)} = \frac{P^{(g)}_{sc}}{P_z}, \quad \eta^{(r)} = \frac{P^{(r)}_{sc}}{P_z},$$

$$\eta = \eta^{(g)} + \eta^{(r)} = \frac{P_{sc}}{P_z}. \quad (14)$$

In general, the goodness of the parameter η for describing the scattering efficiency depends on the type of light source. For example, in the case of a transverse quasiplane wave with a cross section area A in free space, the expression for the propagation power is $P_z=(c\epsilon_0|\mathcal{E}|^2/2)A$. This leads to $\eta=\sigma/A$, where $\sigma=2\hbar\omega\Gamma_{sc}/c\epsilon_0|\mathcal{E}|^2$ is the scattering cross section of the atom. In this case, the use of η as a measure of the scattering efficiency is appropriate. However, in the case of a standing wave in a cavity, we have $P_z=0$. In this case, η becomes infinite and has no physical meaning. We believe that the parameters $\eta^{(g)}$, $\eta^{(r)}$, and η, defined by Eqs. (14), are appropriate characteristics of the scattering efficiency in the case of fibers. The reason is that the essential feature of the field in a fiber is the propagation along the fiber axis.

We emphasize that the confinement of the field in a guided mode with a small effective cross sectional area may allow one to achieve a significant field intensity with a small propagation power, and consequently to achieve substantial scattering efficiencies $\eta^{(g)}$, $\eta^{(r)}$, and η. In addition, the scattering efficiencies can be increased by the fact that the longitudinal field component $\mathcal{E}_0$ and the tangential component S_φ of the Poynting vector contribute to the scattering rates $\Gamma^{(g)}_{sc}$, $\Gamma^{(r)}_{sc}$, and Γ_{sc} but not to the propagation power P_z. Meanwhile, the enhancement of spontaneous emission tends to reduce $\eta^{(g)}$, $\eta^{(r)}$, and η, as discussed in the previous subsection.

The parameters $\eta^{(g)}$, $\eta^{(r)}$, and η are the basic characteristics of light scattering from the atom into guided modes, radiation modes, and both types of modes. It is not easy to measure them directly in experiments. It may be much more convenient to measure the loss of forward guided modes and the scattering into backward guided modes. The scattering rate into backward guided modes is $\Gamma_{back}=\Gamma^{(g)}_{sc}/2$ and the loss rate is $\Gamma_{loss}=\Gamma^{(r)}_{sc}+\Gamma^{(g)}_{sc}/2$. The corresponding powers are $P_{back}=\hbar\omega\Gamma_{back}$ and $P_{loss}=\hbar\omega\Gamma_{loss}$. We introduce the scattering efficiency parameter $\eta_{back}=P_{back}/P_z$ for backward guided modes and the loss parameter $\eta_{loss}=P_{loss}/P_z$ for forward modes. We find the relations

$$\eta_{loss} = \eta^{(r)} + \frac{1}{2}\eta^{(g)},$$

$$\eta_{back} = \frac{1}{2}\eta^{(g)},$$

and

$$\eta^{(r)} = \eta_{loss} - \eta_{back},$$

$$\eta = \eta_{loss} + \eta_{back}.$$

III. NUMERICAL RESULTS

We use Eqs. (12) to calculate the density matrix of the atom interacting with the evanescent light field. For calculations, we choose the fiber radius $a=0.2$ μm. The refractive indices of the fiber and the vacuum clad are $n_1=1.45$ and $n_2=1$, respectively. The light wavelength is at or around the cesium D_2 line wavelength $\lambda_0=852$ nm, and the light polarization is counterclockwise rotating. We consider two different cases where the field intensity in the close vicinity of the fiber surface is well below saturation in one case and near saturation in the other case.

A. Low field intensity

In this subsection, we consider the case where the field intensity is well below saturation. For this regime, we choose, as an example, the propagation power $P_z=10$ fW $=10^{-14}$ W. The corresponding z-axis flux is $n_z=43\times10^3$ s^{-1}. The power chosen here is three orders smaller than the power used for the calculations of Fig. 2. Hence the magnitude of the averaged Poynting vector $\mathbf{S}$ of the field in the close vicinity of the fiber surface is three orders smaller than the saturation intensity I_s for the cesium D_2 line.

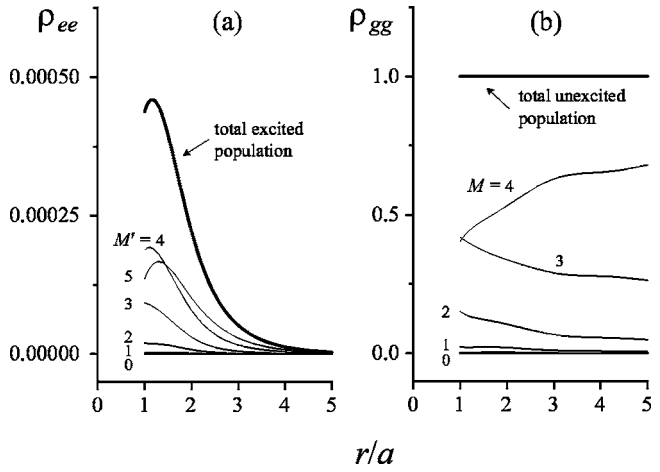

FIG. 4. Spatial dependence of the steady-state populations of (a) the excited sublevels $|F'=5,M'\rangle$ (with $M'=-5,\ldots,5$) and (b) the ground-state sublevels $|F=4,M\rangle$ (with $M=-4,\ldots,4$) for the propagation power $P_z=10$ fW (the z-axis flux $n_z=43\times10^3$ s^{-1}). The total excited population $\Sigma_e\rho_{ee}$ and total unexcited population $\Sigma_g\rho_{gg}$ are shown by thick curves. The field is tuned to exact resonance with the atom. Other parameters are as in Fig. 2. Note that the curves for $M'<0$ and $M<0$ are almost indistinguishable from the curves for $M'=0$ and $M=0$, respectively, because of limited resolution.

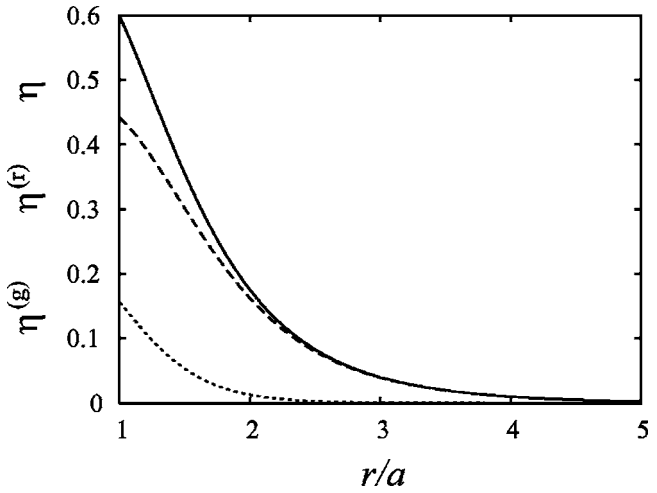

FIG. 5. Spatial dependence of the scattering efficiency parameters η (solid line), $\eta^{(r)}$ (dashed line), and $\eta^{(g)}$ (dotted line) for the case of Fig. 4.

We plot in Fig. 4 the spatial dependence of the steady-state populations of the excited and ground-state sublevels in the case where the field is on exact resonance with the atom. The figure shows that the excited population of the atom is very small [see the small scale of the vertical axis in Fig. 4(a)] and consequently most of the atomic population remains in the ground state [see the thick curve for $\Sigma_g\rho_{gg}$ in Fig. 4(b)]. We observe that the population is not equally distributed with respect to the magnetic quantum numbers M' [see Fig. 4(a)] and M [see Fig. 4(b)]. Although the field is very weak and consequently the excitation is very small, the populations of the sublevels of the ground state are significantly redistributed in the steady state. This redistribution is due to the degeneracy of the ground state and the unequal couplings of the ground-state sublevels with the upper sublevels. Note that the atomic population is concentrated on the magnetic sublevels with positive M' and M. At most spatial locations, the population increases with increasing M' and M. Such a distribution is a result of the competition of the optical pumping processes involving the three different field components $\mathcal{E}_{-1}$, $\mathcal{E}_0$, and $\mathcal{E}_1$, where $|\mathcal{E}_{-1}|>|\mathcal{E}_0|>|\mathcal{E}_1|$. Due to the selection rule and the role of spontaneous emission, the strongest field component $\mathcal{E}_{-1}$ pumps the atom toward the sublevels $M'=5$ and $M=4$ [17]. This effect is reduced by the two weaker components $\mathcal{E}_0$ and $\mathcal{E}_1$, which pump the atom toward the pair $M'=0$ and $M=0$ and the pair $M'=-5$ and $M=-4$, respectively.

In Fig. 5, we plot the spatial dependence of the scattering efficiency parameters η, $\eta^{(r)}$, and $\eta^{(g)}$ for the case of Fig. 4. As seen, the maximal efficiencies, achieved at $r/a=1$, are $\eta\cong0.6$, $\eta^{(r)}\cong0.44$, and $\eta^{(g)}\cong0.16$. They are comparable to each other and to unity. The peak value $\eta\cong0.6$ indicates that, in the close vicinity of the fiber surface, the scattered power P_{sc} is a significant fraction (up to 60%) of the propagation power P_z. Such a high scattering efficiency is due to the specific features of the field in the fundamental mode of the thin fiber. The mechanism is twofold: (i) the confinement of the fiber mode allows a field with a small propagation power P_z to achieve a significant intensity $|\boldsymbol{\mathcal{E}}|^2$ and hence to produce a substantial scattering rate Γ_{sc}, and (ii) the longitudinal component $\mathcal{E}_0$ of the field and the tangential component S_φ of the Poynting vector contribute to the scattering rate Γ_{sc} but not to the propagation power P_z.

The peak value $\eta^{(g)}\cong0.16$ indicates that, in the vicinity of the fiber surface, the power $P_{sc}^{(g)}$ scattered into guided modes can be significant as compared to the total scattered power P_{sc} (up to 26%) and as compared to the total propagation power P_z (up to 16%). Such substantial scattering into guided modes is possible because the rate of spontaneous emission into guided modes $\gamma_{ee}^{(g)}$ in the vicinity of the fiber surface is substantial as compared to the total spontaneous emission rate γ_{ee} (see Fig. 3) [13].

The peak value $\eta^{(r)}\cong0.44$ indicates that, in the vicinity of the fiber surface, the power $P_{sc}^{(r)}$ scattered into radiation modes can be as significant as 44% of the propagation power P_z. With increasing distance from the atom to the fiber, $\eta^{(r)}$ reduces more slowly than $\eta^{(g)}$, and therefore η approaches $\eta^{(r)}$. For $r/a>3$, scattering into guided modes is weak, and scattering into radiation modes is the main scattering mechanism.

In Fig. 6, we plot the tuning characteristics of the scattering efficiency parameters η, $\eta^{(r)}$, and $\eta^{(g)}$ for $r/a=1$ and $r/a=2$. All other parameters are the same as those for Fig. 4. As seen, the three efficiency parameters have almost the same linewidth. The linewidth of 9.4 MHz in Fig. 6(a) is larger than the linewidth of 5.4 MHz in Fig. 6(b). Both linewidths are larger than the natural linewidth of 5.2 MHz for the cesium D_2 line although the power of the field is very low and hence the effect of power broadening is very weak. Such broadening is a signature of the enhancement of spon-

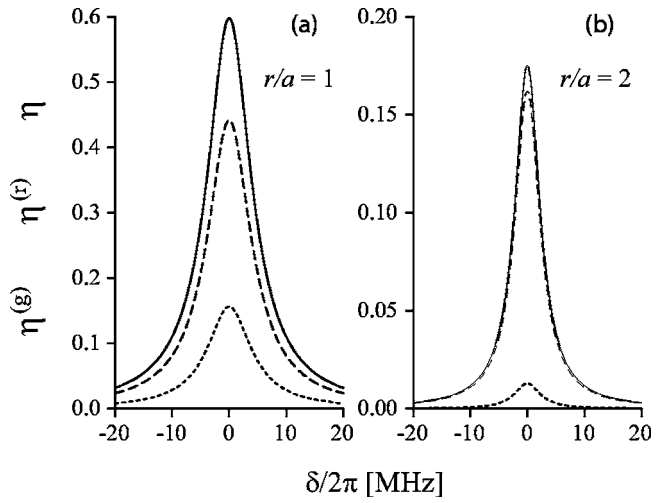

FIG. 6. Tuning characteristics of the scattering efficiency parameters η (solid line), $\eta^{(r)}$ (dashed line), and $\eta^{(g)}$ (dotted line). The position of the atom is (a) $r/a=1$ and (b) $r/a=2$. Other parameters are as for Fig. 4.

taneous emission by the fiber. Hence measuring the linewidth of one of the scattering efficiency parameters $\eta^{(g)}$, $\eta^{(r)}$, and η as a function of space would give us information about the magnitude and spatial dependence of the spontaneous emission characteristics.

To get insight into the loss parameter η_{loss} and the backward scattering efficiency η_{back}, we plot in Fig. 7 the spatial and tuning dependences of these parameters. Their maximal values, achieved at $r/a=1$ and $\delta=0$, are $\eta_{loss}\cong 0.52$ and $\eta_{back}\cong 0.08$. Thus, in the vicinity of the fiber surface, the power P_{loss} of light lost by scattering into radiation modes and backward guided modes can be up to 52% of the propagation power P_z. In other words, the transmittance of the

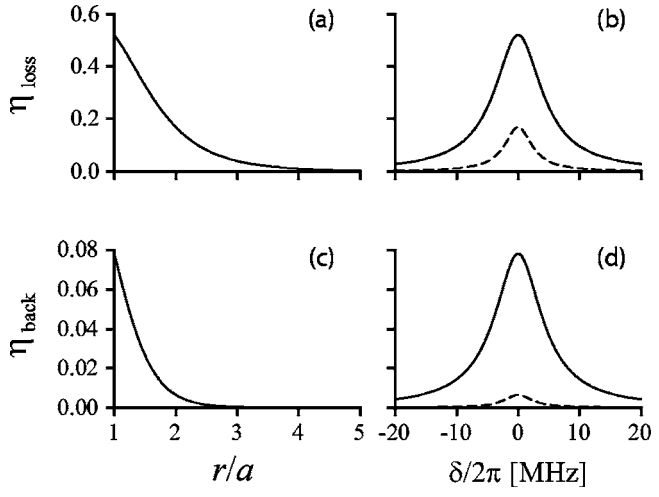

FIG. 7. Left column: spatial dependence of (a) the loss parameter η_{loss} and (c) the backward scattering efficiency η_{back}. The field is tuned to exact resonance with the atom. Right column: tuning characteristics of (b) the loss parameter η_{loss} and (d) the backward scattering efficiency η_{back}. The position of the atom is $r/a=1$ (solid lines) and $r/a=2$ (dashed lines). Other parameters are as for Fig. 4.

field can be reduced to 48%. Meanwhile, the power P_{back} of light scattered into backward guided modes can be up to 8% of P_z. With increasing distance from the atom to the fiber, η_{loss} reduces more slowly than η_{back}. Scattering into backward guided modes becomes very weak for $r/a>3$, while loss due to scattering remains substantial for longer distances. Unlike the spatial profiles, the tuning profiles of η_{loss} and η_{back} have almost the same shape and almost the same linewidth.

According to Ref. [9], the transmittance of a weak field can be reduced to 44%. However, our minimal transmittance is 48%, achieved for the atom on the fiber surface. So, our result is different but not much different from the result of Ref. [9]. The main reason for the difference is that two special important factors, namely the specific structure of the guided field and the enhancement of spontaneous emission, are included in our treatment but not in the treatment of Ref. [9]. The difference is not substantial because the two factors have opposite effects on the scattering efficiency, one increases and the other one decreases.

The propagation power $P_z=10$ fW is small enough that the field can be considered as a perturbation. Our numerical calculations show that any further decrease in P_z would not practically change the steady-state populations ρ_{gg} of the ground-state sublevels as well as the scattering efficiency parameters η, $\eta^{(r)}$, $\eta^{(g)}$, η_{loss}, and η_{back}. Consequently, Fig. 4(b) and Figs. 5–7 remain valid when $P_z\leqslant 10^{-14}$ W. Due to the population redistribution of the ground-state sublevels [see Fig. 4(b)] and the modification of spontaneous emission by the fiber (see Fig. 3), the conventional result (A4) of the perturbation approach [14,20] for the scattering cross section in the steady-state regime cannot be used even though the atomic excitation is weak.

The atom can reach its steady state only when the evolution time t is large as compared to the set of decay times γ_{ee}^{-1} as well as to the set of Rabi periods $|\Omega_{eg}|^{-1}$. Therefore when the propagation power is sufficiently low that the Rabi frequencies $|\Omega_{eg}|$ are smaller than the decay rates γ_{ee}, we may observe two different time scales on which the atomic state evolves. To illustrate this fact, we plot in Fig. 8 the time evolution of the total excited population $\rho_\Sigma=\Sigma_e\rho_{ee}$ for two different ranges of evolution times, $t\leqslant 1$ μs and $t\leqslant 20$ ms. In the calculations for this figure, we assumed that at the initial time $t=0$ the atom was prepared in an incoherent statistical mixture of the ground-state sublevels with equal weight factors, that is, $\rho_{gg'}(0)=\delta_{gg'}/(2F+1)$ and $\rho_{ee'}(0)=\rho_{eg}(0)=0$. We observe that the atom quickly evolves to a quasisteady state [see Fig. 8(a)] and then slowly evolves toward a true steady state [see Fig. 8(b)]. The existence of the two time scales is due to the degeneracy of the ground state and the difference between the Rabi frequency and the decay rate. It is a well-known feature of optical pumping [21]. On the first, shorter time scale, a quasiadiabatic coupling is established for each pair of the ground- and excited-state sublevels without causing any substantial changes in the populations of the ground-state sublevels. The duration of this stage is typically one order larger than the decay times γ_{ee}^{-1}, which are of the same order as γ_0^{-1}. The multilevel atom in this regime can be considered as a set of independent two-level systems. On the second, longer time scale, the

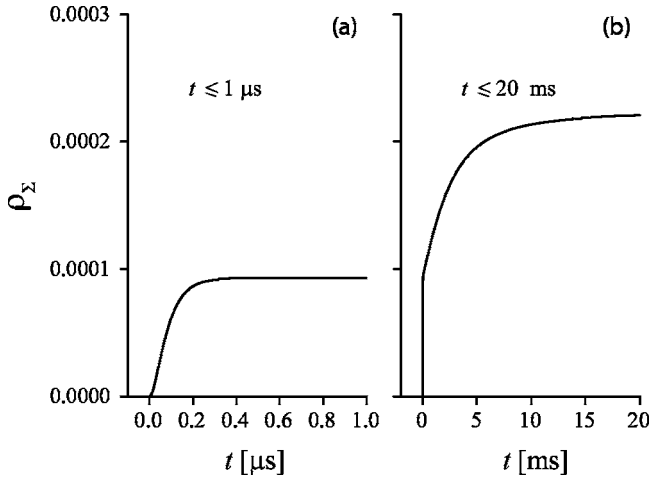

FIG. 8. Time evolution of the total population ρ_Σ of the excited sublevels of the atom. The propagation power is $P_z=10$ fW. The atom is located at the radial distance $r/a=2$. The ranges of interaction times are (a) $t\leqslant 1$ μs and (b) $t\leqslant 20$ ms. Other parameters are as for Fig. 4.

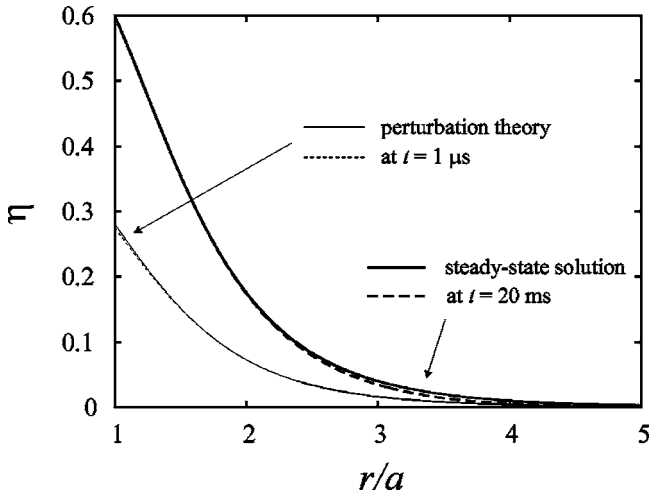

FIG. 9. Spatial dependence of the total scattering efficiency η calculated from the exact time-dependent solution for the atomic state at $t=1$ μs (dotted line) and $t=20$ ms (dashed line). The results of the perturbation theory and the steady-state solution are plotted by the thin and thick solid curves, respectively. Other parameters are as for Fig. 4.

populations of the ground-state sublevels are substantially redistributed [see Fig. 4(b)] due to the combined action of optical pumping and spontaneous emission [21]. The duration of this stage is typically two or three orders greater than the Rabi periods $|\Omega_{eg}|^{-1}$. The degeneracy of the ground state and the competition between different transition channels play an important role in this stage.

At the onset of the quasistationary regime, the populations ρ_{gg} of the ground-state sublevels remain basically unchanged while the atomic polarizations ρ_{eg} already catch up the field. In this regime, we can use the conventional perturbation approach [14,20] to calculate the scattering cross section σ_l for each polarization $l=0,\pm 1$ of the field (see the Appendix). Using this cross section, we can calculate the scattering rate $\Gamma_{sc}=\Sigma_l c\epsilon_0\sigma_l|\mathcal{E}_l|^2/2\hbar\omega$ and hence the scattering efficiency η of the atom. We plot in Fig. 9 the spatial dependence of the total scattering efficiency η for the transient atomic states established at $t=1$ μs, corresponding to the onset of the quasistationary regime, and at $t=20$ ms, corresponding to the onset of the steady-state regime. The figure shows that the results for the onset of the quasistationary regime (dotted curve) almost coincide with the results of the conventional perturbation approach.

B. Substantial field intensity

In this subsection, we study the case where the field intensity is near saturation. For this regime, we choose the propagation power $P_z=10$ pW$=10^{-11}$ W. The corresponding z-axis flux is $n_z=43\times 10^6$ s^{-1}. Although the power chosen is small, the averaged Poynting vector of the field in the close vicinity of the fiber surface is, as shown in Fig. 2(b), on the order of the saturation intensity $I_s=1.1$ mW/cm^2.

We plot in Fig. 10 the spatial dependence of the steady-state populations of the excited and ground-state sublevels. The figure shows that the effect of optical pumping on the atomic population distribution is strong. Indeed, a significant fraction of the total population is now in the excited sublevels.

In Fig. 11, we plot the spatial dependence of the scattering efficiency parameters η, $\eta^{(r)}$, and $\eta^{(g)}$ for the case of Fig. 10. We observe that, in the close vicinity of the fiber surface, the power scattered into guided modes, the power scattered into radiation modes, and the total scattered power can be as significant as 8%, 24%, and 32%, respectively, of the propagation power.

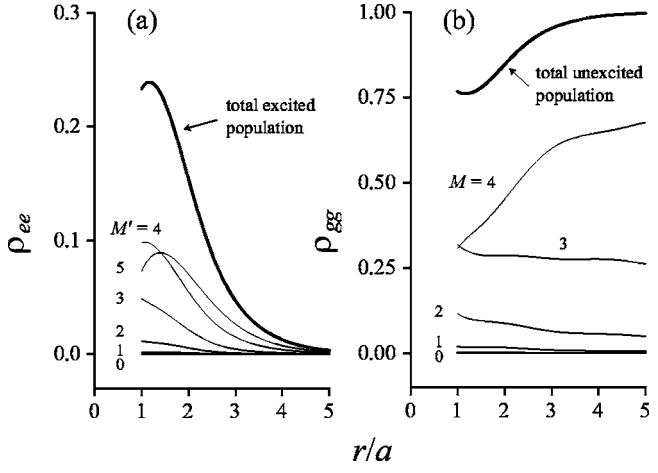

FIG. 10. Spatial dependence of the steady-state populations of (a) the excited sublevels $|F'=5,M'\rangle$ (with $M'=-5,\ldots,5$) and (b) the ground-state sublevels $|F=4,M\rangle$ (with $M=-4,\ldots,4$) for the propagation power $P_z=10$ pW (the z-axis flux $n_z=43\times 10^6$ s^{-1}). The total excited population $\Sigma_e\rho_{ee}$ and total unexcited population $\Sigma_g\rho_{gg}$ are shown by thick curves. The field is tuned to exact resonance with the atom. Other parameters are as in Fig. 2. Note that the curves for $M'<0$ and $M<0$ are almost indistinguishable from the curves for $M'=0$ and $M=0$, respectively, because of limited resolution.

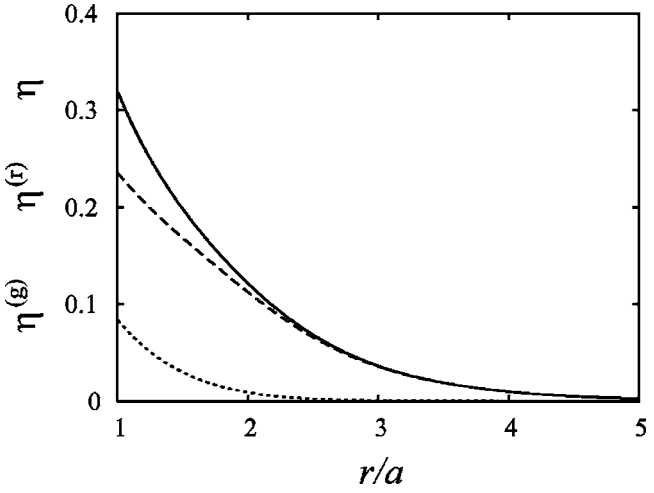

FIG. 11. Spatial dependence of the scattering efficiency parameters η (solid line), $\eta^{(r)}$ (dashed line), and $\eta^{(g)}$ (dotted line) for the case of Fig. 10.

In Fig. 12, we plot the tuning characteristics of the scattering efficiency parameters η, $\eta^{(r)}$, and $\eta^{(g)}$ for $r/a=1$ and $r/a=2$. The linewidths observed in Figs. 12(a) and 12(b) are about 13 and 6.5 MHz, respectively. They are slightly larger than the corresponding linewidths in Fig. 6. Such increase is due to the power broadening effect.

We plot in Fig. 13 the spatial and tuning dependences of the loss parameter η_{loss} and the backward scattering efficiency η_{back}. The figure shows that, in the vicinity of the fiber surface, the power of light lost from forward direction by scattering into radiation modes and backward guided modes can be up to 28% of the propagation power, and the power scattered into backward guided modes can be up to 4% of the propagation power.

Comparison between Figs. 5–7 and 11–13 shows that a dramatic increase in the propagation power from 10 fW to 10 pW leads to a minor decrease in the scattering efficiency.

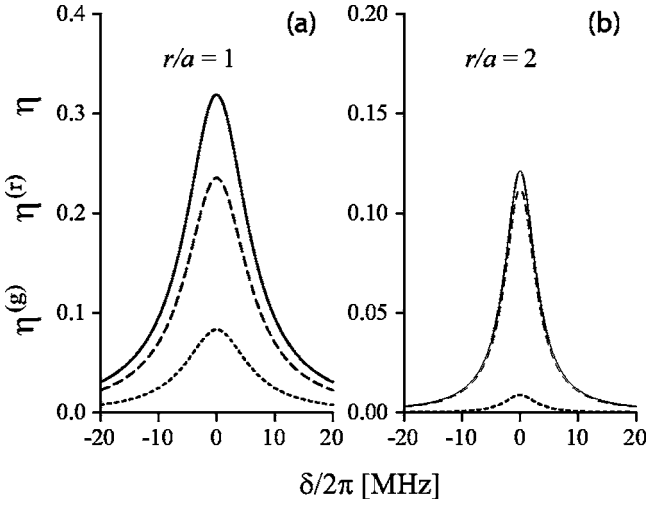

FIG. 12. Tuning characteristics of the scattering efficiency parameters η (solid line), $\eta^{(r)}$ (dashed line), and $\eta^{(g)}$ (dotted line). The position of the atom is (a) $r/a=1$ and (b) $r/a=2$. Other parameters are as for Fig. 10.

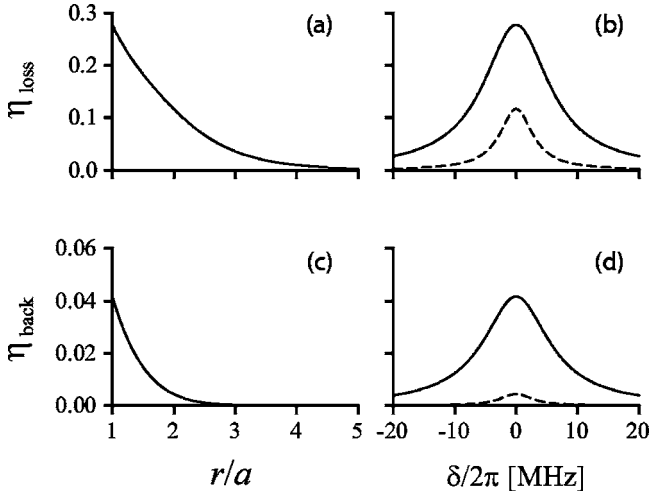

FIG. 13. Left column: spatial dependence of (a) the loss parameter η_{loss} and (c) the backward scattering efficiency η_{back}. The field is tuned to exact resonance with the atom. Right column: tuning characteristics of (b) the loss parameter η_{loss} and (d) the backward scattering efficiency η_{back}. The position of the atom is $r/a=1$ (solid lines) and $r/a=2$ (dashed lines). Other parameters are as for Fig. 10.

Due to the saturation effect, a further increase in the propagation power will lead to a dramatic decrease in the scattering efficiency. Therefore we are not interested in the case of higher powers.

IV. CONCLUSIONS

We have studied the scattering of an evanescent light field by a cesium atom outside a subwavelength-diameter fiber. We have shown that the confinement of the field, the presence of the longitudinal field component and the tangential Poynting vector component, the enhancement of spontaneous emission, and the degeneracy of the cesium ground state substantially affect the scattering process. In the vicinity of the fiber surface, the scattering efficiency, determined as the ratio of the scattered power to the propagation power, can be as significant as 16% for scattering into guided modes, 44% for scattering into radiation modes, and hence 60% for the total scattering. Hence the transmittance of the field in the stationary regime can be substantially reduced to 48% due to scattering into radiation modes (44%) and backward guided modes (8%). The scattering efficiency is substantial because (i) the confinement of the fiber mode allows the field to achieve a significant intensity with a small propagation power, and (ii) the longitudinal component of the field and the tangential component of the Poynting vector contribute to the scattering rate but not to the propagation power. The scattering into guided modes is significant because the spontaneous emission into guided modes is a substantial fraction of the total spontaneous emission from the atom. We have numerically demonstrated that, in the case of low propagation powers, due to the degeneracy of the ground state, there are two different time scales on which the atomic state evolves. In the first, shorter time regime, a quasiadiabatic

coupling is established for each pair of the ground- and excited-state sublevels without causing any substantial changes in the populations. In the second, longer time regime, the populations of the ground-state sublevels are substantially redistributed due to the combined action of optical pumping and spontaneous emission. The existence of the two time scales is a well-known feature of optical pumping [21]. We recognize that a more accurate description for a weak field would require us to take into account the quantum nature of the field. This will be the subject of a future work.

ACKNOWLEDGMENTS

This work was carried out under the 21st Century COE program on "Coherent Optical Science."

APPENDIX: SCATTERING CROSS SECTION OF AN ATOM IN THE FRAMEWORK OF THE PERTURBATION THEORY

We consider a single atom interacting with a continuous-wave field $\mathbf{E}=(\mathcal{E}\boldsymbol{\epsilon}e^{-i\omega t}+\mathcal{E}^{*}\boldsymbol{\epsilon}^{*}e^{i\omega t})/2$. Here $\mathcal{E}$, $\boldsymbol{\epsilon}$, and ω are the complex amplitude, polarization vector, and angular frequency of the field, respectively. We first examine the case where the atom has only two energy levels, called the ground state $|g\rangle$ and the upper state $|e\rangle$. In this case, the scattering cross section of the atom is given by [8]

$$\sigma=\frac{\omega}{2\epsilon_0\hbar c}\frac{\gamma_e|d_{eg}|^2}{(\omega-\omega_{eg})^2+\gamma_e^2/4+|\Omega_{eg}|^2/2}. \tag{A1}$$

Here $\omega_{eg}=\omega_e-\omega_g$ is the angular transition frequency, $d_{eg}=\langle e|\boldsymbol{\epsilon}\cdot\mathbf{d}|g\rangle$ is the dipole-moment matrix element, $\Omega_{eg}=d_{eg}\mathcal{E}/\hbar$ is the Rabi frequency, and γ_e is the linewidth determined by the population decay rate of the upper state (twice the dephasing rate). The cross section σ represents the power scattered per atom for a unit incident energy flux. The scattering rate Γ_{sc} is related to σ through

$$\Gamma_{\mathrm{sc}}=\frac{\sigma I}{\hbar\omega}=\frac{c\epsilon_0\sigma|\mathcal{E}|^2}{2\hbar\omega}, \tag{A2}$$

where $I=c\epsilon_0|\mathcal{E}|^2/2$ is the intensity of the laser beam. The absorption coefficient α of a bulk medium with N atoms per unit volume is related to σ as $\alpha=N\sigma$.

The presence of Ω_{eg} in Eq. (A1) is a consequence of the power broadening effect. The saturation intensity is determined from the condition $|\Omega_{eg}|=\gamma_e/\sqrt{2}$ and is given by $I_s=c\epsilon_0\hbar^2\gamma_e^2/4|d_{eg}|^2$. For the transition $J_g=0\leftrightarrow J_e=1$, we have $\gamma_e=\omega_{eg}^3|\langle e\|d\|g\rangle|^2/9\pi\epsilon_0\hbar c^3$ and $|d_{eg}|=|\langle e\|d\|g\rangle|/\sqrt{3}$, leading to $\gamma_e=\omega_{eg}^3|d_{eg}|^2/3\pi\epsilon_0\hbar c^3$. Then, the saturation intensity becomes $I_s=2\pi^2\hbar c\gamma_e/3\lambda_{eg}^3$. Here, $\lambda_{eg}=2\pi c/\omega_{eg}$ is the transition wavelength and $\langle e\|d\|g\rangle$ is the reduced electric dipole matrix element.

When the Rabi frequency Ω_{eg} of the field is small as compared to the decay rate γ_e, the effect of power broadening in Eq. (A1) can be neglected. In this case, we have

$$\sigma=\frac{\omega}{2\epsilon_0\hbar c}\frac{\gamma_e|d_{eg}|^2}{(\omega-\omega_{eg})^2+\gamma_e^2/4}. \tag{A3}$$

At exact resonance ($\omega=\omega_{eg}$), Eq. (A3) reduces to $\sigma=2\omega_{eg}|d_{eg}|^2/\epsilon_0\hbar c\gamma_e$. For $\gamma_e=\omega_{eg}^3|d_{eg}|^2/3\pi\epsilon_0\hbar c^3$, the on-resonance cross section becomes $\sigma=3\lambda_{eg}^2/2\pi$.

We now consider the case of a multilevel atom with a degenerate lower state and a degenerate upper state. More concretely, we consider an alkali atom with magnetic sublevels $|M\rangle\equiv|FM\rangle\equiv|LSJIFM\rangle$ of a hyperfine-structure level F of the ground state $|LJ\rangle$ and magnetic sublevels $|M'\rangle\equiv|F'M'\rangle\equiv|L'SJ'IF'M'\rangle$ of a hyperfine-structure level F' of the upper state $|L'J'\rangle$. Here, the quantum numbers L, L', J, J', F, F', S, and I are fixed. The quantization axis is the z axis. We assume that the atom is initially prepared in an incoherent mixture of the magnetic sublevels $|M\rangle$ and that the initial population distribution of the atom is flat with respect to M. We introduce the spherical tensor notation $\mathbf{u}_0=\hat{\mathbf{z}}$ and $\mathbf{u}_{\pm1}=\mp(\hat{\mathbf{x}}\pm i\hat{\mathbf{y}})/\sqrt{2}$. The vector $\mathbf{u}_0$ describes linear polarization, and the vectors $\mathbf{u}_1$ and $\mathbf{u}_{-1}$ describe left and right circular polarizations, respectively.

We assume that the characteristic Rabi frequency of the field is small as compared to the characteristic decay rate. We consider the regime in which the interaction time is large enough as compared to the characteristic decay time but is small as compared to the characteristic Rabi period. Under these conditions, the effect of optical pumping is small and, consequently, the redistribution of atomic level populations is negligible, while the atomic state evolves slowly in time. In this case, the quasistationary scattering cross section of the atom can be obtained by summing up expression (A3) over the upper magnetic sublevels $|M'\rangle$ and averaging the result over the lower magnetic sublevels $|M\rangle$. Then, with the use of Eq. (6), we find the following expression for the quasistationary cross section:

$$\sigma_l=\frac{\omega}{2\epsilon_0\hbar c}|\langle J'\|D\|J\rangle|^2\sum_{MM'}(2F'+1)\times\begin{Bmatrix}J' & F' & I\\ F & J & 1\end{Bmatrix}^2\begin{pmatrix}F & 1 & F'\\ M & l & -M'\end{pmatrix}^2\times\frac{\gamma_{M'}}{(\omega-\omega_{M'M})^2+\gamma_{M'}^2/4}. \tag{A4}$$

Here, the integer index $l=-1$, 0, or $+1$ specifies the field polarization. When the polarization of the field is arbitrary, the quasistationary scattering rate Γ_{sc} is given by

$$\Gamma_{\mathrm{sc}}=\sum_{l=0,\pm1}\frac{c\epsilon_0\sigma_l|\mathcal{E}_l|^2}{2\hbar\omega}. \tag{A5}$$

In free space, the transition frequency $\omega_{M'M}$ does not depend on the magnetic quantum numbers M' and M, that is, $\omega_{M'M}=\omega_0$, and the natural linewidth does not depend on M', that is, $\gamma_{M'}=\gamma_0$. Then, the summation over M and M' in expression (A4) applies only to the $3j$ symbols and can be simplified. This leads to

$$\sigma_l = \sigma = \frac{\omega}{6\epsilon_0 \hbar c} |\langle J' \| D \| J \rangle|^2 (2F' + 1) \begin{Bmatrix} J' & F' & I \\ F & J & 1 \end{Bmatrix}^2 \times \frac{\gamma_0}{(\omega - \omega_0)^2 + \gamma_0^2/4}. \quad \text{(A6)}$$

Using the above expression, we estimate that the on-resonance scattering cross section is about 0.14 μm^2.

We note that Eq. (A6) is independent of the field polarization index l. This expression can be obtained from the imaginary part of the complex susceptibility in the conventional perturbation approach [20]. Similar expressions have been obtained and used to study the absorption properties of cesium [14].

We emphasize that the above result is valid only for the quasistationary regime, where the population redistribution is negligible. When the atom approaches its steady state, the degeneracy of the ground state and the unequal couplings of the ground-state sublevels with the upper sublevels require the populations of the ground-state sublevels to redistribute. Therefore Eq. (A4) cannot be used for the scattering cross section of the cesium atom in the steady-state regime even if the field is weak.

[1] L. Tong, R. R. Gattass, J. B. Ashcom, S. He, J. Lou, M. Shen, I. Maxwell, and E. Mazur, Nature (London) **426**, 816 (2003).

[2] T. A. Birks, W. J. Wadsworth, and P. St. J. Russell, Opt. Lett. **25**, 1415 (2000); S. G. Leon-Saval, T. A. Birks, W. J. Wadsworth, P. St. J. Russell, and M. W. Mason, *Conference on Lasers and Electro-Optics (CLEO)*, Technical Digest, Postconference Edition (Optical Society of America, Washington, DC, 2004), paper CPDA6.

[3] V. I. Balykin, K. Hakuta, F. L. Kien, J. Q. Liang, and M. Morinaga, Phys. Rev. A **70**, 011401(R) (2004).

[4] Fam Le Kien, V. I. Balykin, and K. Hakuta, Phys. Rev. A **70**, 063403 (2004).

[5] N. Schlosser, G. Reymond, I. Protsenko, and P. Grangier, Nature (London) **411**, 1024 (2001).

[6] S. Kuhr, W. Alt, D. Schrader, M. Müller, V. Gomer, and D. Meschede, Science **293**, 278 (2001).

[7] C. A. Sackett, D. Kielpinski, B. E. King, C. Langer, V. Meyer, C. J. Myatt, M. Rowe, Q. A. Turchette, W. M. Itano, D. J. Wineland, and C. Monroe, Nature (London) **404**, 256 (2000).

[8] See, for example, R. Loudon, *The Quantum Theory of Light* (Oxford, New York, 1983).

[9] P. Domokos, P. Horak, and H. Ritsch, Phys. Rev. A **65**, 033832 (2002).

[10] L. Tong, J. Lou, and E. Mazur, Opt. Express **12**, 1025 (2004).

[11] Fam Le Kien, J. Q. Liang, K. Hakuta, and V. I. Balykin, Opt. Commun. **242**, 445 (2004).

[12] H. Nha and W. Jhe, Phys. Rev. A **56**, 2213 (1997); T. Søndergaard and B. Tromborg, *ibid.* **64**, 033812 (2001); V. V. Klimov and M. Ducloy, *ibid.* **69**, 013812 (2004).

[13] Fam Le Kien, S. Dutta Gupta, V. I. Balykin, and K. Hakuta, Phys. Rev. A **72**, 032509 (2005).

[14] R. J. Rafac and C. E. Tanner, Phys. Rev. A **58**, 1087 (1998); I. Hirano, *ibid.* **50**, 4650 (1994); S. Tojo, M. Hasuo, and T. Fujimoto, Phys. Rev. Lett. **92**, 053001 (2004).

[15] Fam Le Kien, V. I. Balykin, and K. Hakuta, J. Phys. Soc. Jpn. **74**, 910 (2005).

[16] See, for example, D. Marcuse, *Light Transmission Optics* (Krieger, Malabar, FL, 1989).

[17] H. J. Metcalf and P. van der Straten, *Laser Cooling and Trapping* (Springer, New York, 1999).

[18] See, for example, B. W. Shore, *The Theory of Coherent Atomic Excitation* (Wiley, New York, 1990).

[19] S. Chang and V. Minogin, Phys. Rep. **365**, 65 (2002).

[20] See, for example, R. W. Boyd, *Nonlinear Optics* (Academic, New York, 1992).

[21] T. G. Walker and W. Happer, Rev. Mod. Phys. **69**, 629 (1997).